Astro-E/XRS blocking filter calibration

Michael D. Audley[a], Keith A. Arnaud[b,c], Keith C. Gendreau[b,c], Kevin R. Boyce[c], Charles M. Fleetwood[c], Richard L. Kelley[c], Ritva A. Keski-Kuha[c], F. Scott Porter[c], Caroline K. Stahle[c], Andrew E. Szymkowiak[c], June L. Tveekrem[c], Ryuichi Fujimoto[a], Kazuhisa Mitsuda[a], Yoshitaka Ishisaki[d], and Tatehiro Mihara[e]

[a]Institute of Space and Astronautical Science, Sagamihara, Kanagawa, Japan

[b]University of Maryland, College Park, MD, USA

[c]NASA / Goddard Space Flight Center, Greenbelt, MD, USA

[d]Tokyo Metropolitan University, Japan

[e]The Institute of Physical and Chemical Research (RIKEN), Japan

ABSTRACT

We describe the transmission calibration of the Astro-E XRS blocking filters. The XRS instrument has five aluminized polymide blocking filters. These filters are located at thermal stages ranging from 200 K to 60 mK. They are each about 1000 Å thick. XRS will have high energy resolution which will enable it to see some of the extended fine structure around the oxygen and aluminum K edges of these filters. Thus, we are conducting a high spectral resolution calibration of the filters near these energies to resolve out extended fine structure and absorption lines.

Keywords: X-ray, Calibration, Optical Blocking Filter, Calorimeter, XRS, ASTRO-E

1. INTRODUCTION

The US-Japanese ASTRO-E observatory is scheduled to be launched in early 2000.[1] ASTRO-E carries four X-ray CCD detectors and a hard X-ray detector. The CCDs are located at the focus of grazing incidence X-ray mirrors and will primarily provide imaging over a 0.4–12 keV bandpass. ASTRO-E also carries the XRS microcalorimeter X-ray detector.[2] The X-Ray Telescope (XRT), a conical X-ray mirror with platinum foils, will focus X-rays onto a 32-element array of microcalorimeter pixels for high-throughput, high-resolution spectroscopy with limited spatial resolution. The mean measured energy resolution of the XRS flight model detector is better than 12 eV at 6 keV for the nominal operating temperature of 60 mK.[3]

The low energy detection efficiency of XRS is determined by thermal/optical blocking filters located along the various thermal stages of the instrument. There are five aluminized polyimide filters with nominal composition listed in Table 1. The XRS filters were manufactured by Luxel Corporation. The composition of the actual flight filters is shown in Table 2.

Along with these five filters, the XRT has a thermal shield. The XRT thermal shield consists of a 0.2 μm layer of PET ($C_{10}H_8O_4$; Toray Lumirror), and 0.03 μm of aluminum The thermal shield is supported by a stainless steel mesh structure 0.15 mm thick with a transmission of 93.4%.

XRS's high spectral resolution makes us sensitive to fine structure in the X-ray absorption edges of the filters as shown in Figure 1 for the oxygen and aluminum edges around 0.5 and 1.5 keV. Thus, it is important that we measure these features on the ground.

2. EXPERIMENTAL SETUP

For early measurements of the engineering model filter IVCS 108 we used a Surface Normal Reflection Monochromator (SNR[5]) manufactured by Hettrick Scientific. We switched to a Hettrick Edge Spectrometer as soon as it became available.

Further author information: (Send correspondence to M.D.A.)
WWW: http://lheawww.gsfc.nasa.gov/users/audley/calibration/
E-mail: audley@astro.isas.ac.jp

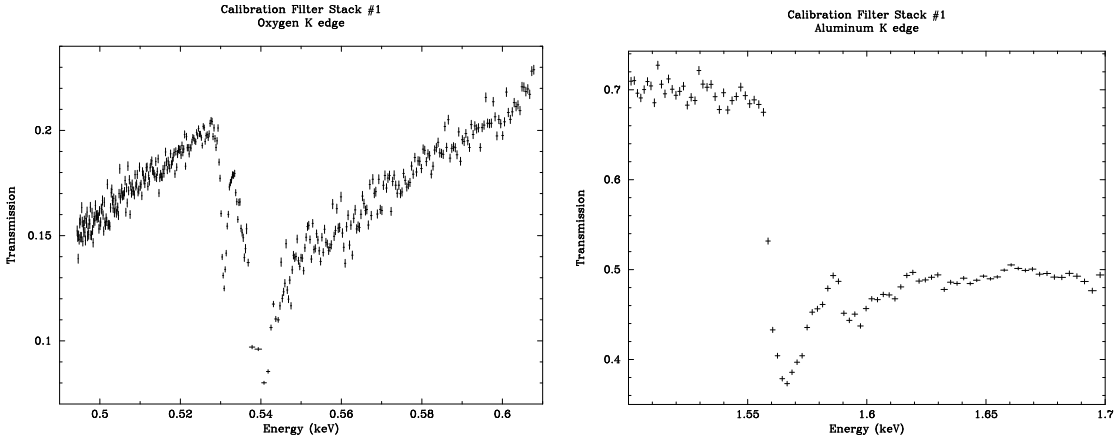

Figure 1. Fine structure near edges measured with the Edge Spectrometer. Left: Oxygen K edge. The $2p\ ^3P^o$ resonance feature near 530 eV is about 2 eV higher in energy than the theoretical value,[4] possibly because of a chemical shift. Right: Aluminum K edge.

Table 1. Nominal composition of the XRS filters.

Filter	Aluminum thickness (Å)	Polyimide thickness (Å)	Mesh
Dewar Main Shell (DMS)	800	1000	70 lines/inch Ni (82% covering factor)
Inner Vacuum Can Shield (IVCS)	1000	1000	none
Solid Neon Tank (Neon)	1000	1000	none
Front End Assembly (FEA)	500	750	none
Cold Temperature Stage (CTS)	500	750	none
Totals	3800	4500	82% covering

2.1. The Edge Spectrometer

The Edge spectrometer (ES) is similar in design to the EUVE spectrometer[6].[7] X-Rays from the entrance slit are reflected by a spherical mirror and then a variable-spacing grating, forming a dispersed image at the focus as shown in Figure 2.

The X-ray source is a Manson source with a horizontal slit in front of it. Slits ranging in width between 5 and 50 μm can be selected. For most of our measurements we use the 20 μm slit as it provides acceptable spectral resolution combined with reasonable throughput.

The detector at the focus of the Edge Spectrometer is an ASCA engineering model CCD which is 1 cm square with 420×420 pixels. The energy resolution of the CCD ($\sim$ 120 eV at 5.9 kev, nominal) allows us to seperate the orders in the dispersed image (see Figure 3).

The image is rotated so that the slit images are parallel to the CCD rows and a PHA spectrum is extracted for each row. Each spectrum is then fitted for first through fourth order intensity. We derive a wavelength solution using characteristic lines that are on top of the continuum from our Manson source and use it to determine the X-ray energy corresponding to each row. The bright O Kα and Au Mζ lines near the oxygen and aluminum edges, respectively, allow us to measure the fine structure in these edges with good counting statistics.

There is an aluminum optical blocking filter between the grating and the CCD. This prevents UV light from the source from contaminating the image.

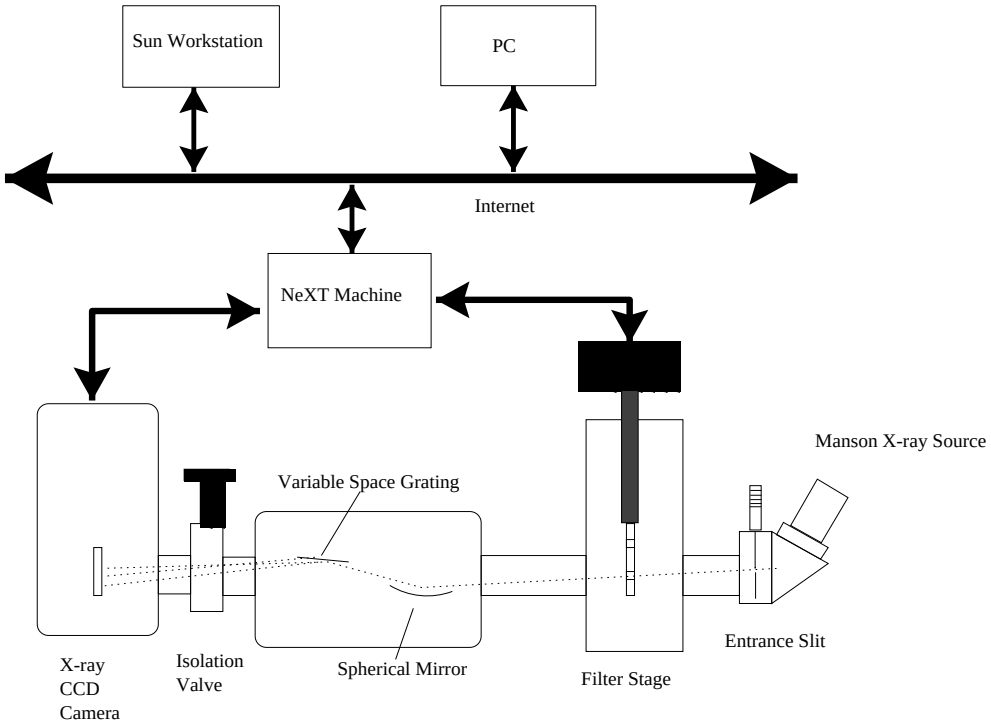

Figure 2. Schematic of the Hettrick Scientific Edge Spectrometer.

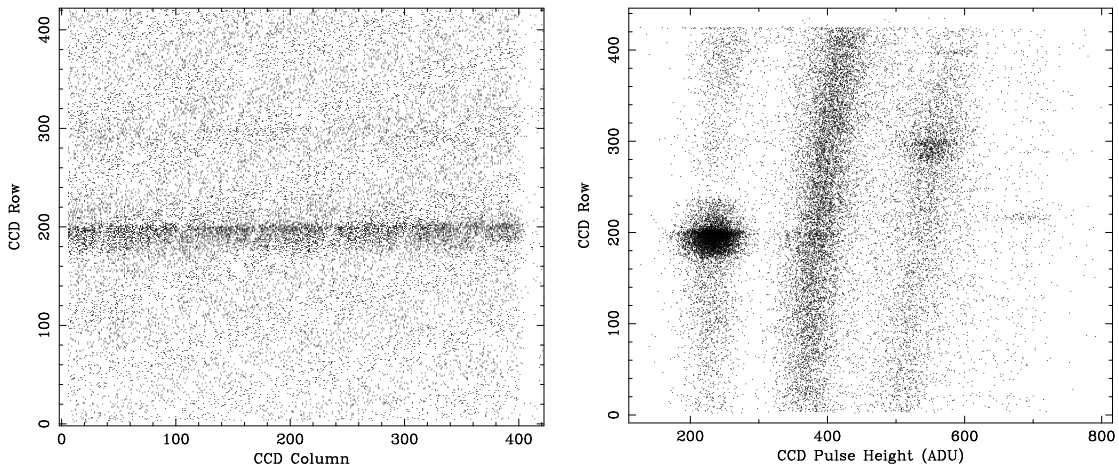

Figure 3. CCD image and order separation. On the left is a CCD image obtained with Neon filter #106 in the Edge Spectrometer. The shadow of the mesh in the Al blocking filter of the ES is visible. On the right, the row and pulse height of each event have been plotted, resolving the data into four spectral orders. The bright oxygen Kα line and K-edge are visible in first order with a pulse height of about 200. Au Mζ is visible in third order near row 300. Au Mα appears in fourth order near row 210.

Table 2. Actual composition of the XRS flight filters based on Luxel-measured thicknesses and measurements of a DMS mesh sample at GSFC. The uncertainties in the individual polyimide and aluminum thicknesses are 100 Å and 50 Å, respectively. The mesh parameters are thickness (t), width (w), and pitch (p).

Filter	Aluminum thickness (Å)	Polyimide thickness (Å)	Ni Mesh Geometry (μm)
DMS 156	874	1065	$t = 18.2 \pm 1.6$ $w = 37.5 \pm 1.2$ $p = 344.17$
IVCS 143	1050	995	none
Neon 146	1050	995	none
FEA 144	510	710	none
CTS 01	495	760	none
Totals	3979 ± 225	4525 ± 110	as for DMS 156

Because the CCD has a 4 s integration time in imaging mode, pileup can be a problem. Usually it is caused by a bright O Kα line, although for high beam currents, the Au Mζ_1 and Mζ_2 lines can also cause pileup. We have taken several measures to eliminate this problem. Targets are generally made of aluminum and coated with gold in an evaporation chamber. We install targets straight from the evaporation chamber to the source and then make sure that the Edge Spectrometer is well-evacuated before warming up the source. To make this easier there is a turbomolecular pump mounted right under the source. An external cooling fan also helps by cooling the source and thus keeping the pressure down in the vacuum chamber.

2.2. The Filter Holder

The filter is in a specially-designed holder which is held on a motorized linear translation stage. This stage moves the filter in and out of the X-ray beam. Operation is completely automatic, allowing data to be collected 24 hours a day. Each CCD frame has an integration time of 4 s. We generally take 250 frames of data with the test filter in the beam and another 250 frames with the test filter out of the beam. This is repeated until enough data have been collected (usually in about a week). This approach minimizes the effects of source variations. In any case, we have found that the intensity of the Manson sources varies by only a few percent on a timescale of months. The filter holder is between the source's slit and the spherical mirror. The beam size here is about 200×20 μm. There was no time to measure the transmission at more than one place on each filter. However, the GSFC Optics Branch measured the filters at 5 different positions (see Section 2.3).

2.3. Measurements by GSFC Optics Branch

For all the filters except IVCS #97 and Neon #106 we had transmission data provided by the GSFC Optics Branch. For these measurements a Manson source was used with different targets to produce fluorescent lines, except for the 5.9 keV data which were obtained with a ^{55}Fe source. The X-rays were detected with a proportional counter. A motorized filter holder chopped the filter in and out of the beam. Each filter was measured at five different positions, separated by 0.025". The beam size was a few mm^2.

3. RESULTS

We ran a measurement of the transmission of an engineering model IVCS filter (IVCS 108) with the SNR continuously for three months starting in May 1998. In that time the beam current of the SNR's Manson source varied by only a few percent. In the first week of February 1999 we measured the engineering model filter IVCS 97 in the ES. We measured flight model filters in the ES from mid-February 1999 until mid-April 1999, when they were delivered to Japan for installation. We typically spent one week measuring a filter in the ES. The flight CTS filter was not available as it was already installed in XRS but the other four flight filters were measured. Then we measured the transmissions of a sample of the XRT thermal shield and a stack of calibration filters.

3.1. Comparison with Expected Transmission

From the Luxel-quoted polyimide and aluminum thicknesses we calculated the expected areal densities for carbon, nitrogen, oxygen, and aluminum for each filter. These are shown in Table 3. To fit for these areal densities in the filter data we used the Henke absorption coefficients[8] and excluded data close to the oxygen and aluminum absorption edges where there is fine structure. In the case of filter IVCS #108 we had both Edge Spectrometer and SNR data which we combined (see Figure 5).

Table 3. Expected areal densities of the XRS filters. These were calculated from the thickness measurements provided by Luxel. The silicon thickness was taken as 1% of the aluminum thickness. Errors were calculated assuming uncertainties of ±50 Å and ±100 Å in the aluminum and polyimide thicknesses, respectively. We assumed densities of 1.44 g cm^{-3} for polyimide, 2.5 g cm^{-3} for aluminum, and 2.32 g cm^{-3} for silicon.

Filter	Aluminum σ (μg cm^{-2})	Carbon σ (μg cm^{-2})	Nitrogen σ (μg cm^{-2})	Oxygen σ (μg cm^{-2})	Silicon σ (μg cm^{-2})
DMS 138	21.0 ± 1.3	10.9 ± 1.0	1.16 ± 0.11	2.64 ± 0.25	0.194 ± 0.012
DMS 139	21.0 ± 1.3	10.3 ± 1.0	1.09 ± 0.11	2.49 ± 0.25	0.194 ± 0.012
DMS 156 (Flight)	21.9 ± 1.3	11.1 ± 1.0	1.17 ± 0.11	2.68 ± 0.25	0.203 ± 0.012
IVCS 97	24.8 ± 1.3	10.4 ± 1.0	1.10 ± 0.11	2.52 ± 0.25	0.230 ± 0.012
IVCS 108	25.1 ± 1.3	11.2 ± 1.0	1.18 ± 0.11	2.71 ± 0.25	0.233 ± 0.012
IVCS 114	25.5 ± 1.3	10.5 ± 1.0	1.11 ± 0.11	2.54 ± 0.25	0.237 ± 0.012
IVCS 123	26.1 ± 1.3	10.6 ± 1.0	1.13 ± 0.11	2.57 ± 0.25	0.242 ± 0.012
IVCS 143 (Flight)	26.3 ± 1.3	10.3 ± 1.0	1.10 ± 0.11	2.50 ± 0.25	0.244 ± 0.012
Neon 106	24.6 ± 1.3	10.4 ± 1.0	1.11 ± 0.11	2.53 ± 0.25	0.229 ± 0.012
Neon 119	25.6 ± 1.3	10.6 ± 1.0	1.13 ± 0.11	2.58 ± 0.25	0.238 ± 0.012
Neon 146 (Flight)	26.3 ± 1.3	10.3 ± 1.0	1.10 ± 0.11	2.50 ± 0.25	0.244 ± 0.012
Neon 153	27.4 ± 1.3	11.2 ± 1.0	1.18 ± 0.11	2.71 ± 0.25	0.254 ± 0.012
FEA 116	13.1 ± 1.3	8.2 ± 1.0	0.86 ± 0.11	1.98 ± 0.25	0.122 ± 0.012
FEA 117	13.1 ± 1.3	8.2 ± 1.0	0.86 ± 0.11	1.98 ± 0.25	0.122 ± 0.012
FEA 144 (Flight)	12.8 ± 1.3	7.4 ± 1.0	0.78 ± 0.11	1.79 ± 0.25	0.118 ± 0.012
Calibration Stack 1	96.1 ± 3.0	48.9 ± 2.3	5.19 ± 0.25	11.85 ± 0.57	0.891 ± 0.028

When we assumed that the Ni mesh of the DMS filter was optically thick, with a transmission fixed at 82% we found that the O Kα edge transmission of the Calibration Filter Stack was only 50% of the expected value.

Using a ^{241}Am α-particle source to excite fluorescent X-ray lines in varous targets, we measured the X-ray transmission of a sample of the DMS Ni mesh provided by Luxel. The mesh thickness and pitch were determined from microscope measurements. The mesh transmission is shown in Figure 4. Clearly our previous assumption that the mesh is optically thick to X-rays was incorrect. The mesh transmission data were then fitted to a function of the form

$$M(E) = \left(\frac{p-w}{p}\right)^2 + \left(1 - \left(\frac{p-w}{p}\right)^2\right) \exp\left(\frac{-t}{\alpha_{\rm Ni}(E)}\right) \quad (1)$$

where the pitch, p, was held fixed. This model assumes that the mesh wires have a rectangular cross-section, which may not be true. Thus, the mesh width, w, and thickness, t, were allowed to vary in the fit. The best-fit values were $t = 18.2 \pm 1.6$ μm and $w = 37.5 \pm 1.2$ μm, with the pitch, p, fixed at the measured value of 344.17 μm.

For fitting the filter transmissions a function of the form

$$T(E) = M(E)\, \exp(-\mu_{\rm C}\sigma_{\rm C})\, \exp(-\mu_{\rm N}\sigma_{\rm N})\, \exp(-\mu_{\rm O}\sigma_{\rm O})\, \exp(-\mu_{\rm Si}\sigma_{\rm Si})\, \exp(-\mu_{\rm Al}\sigma_{\rm Al}) \quad (2)$$

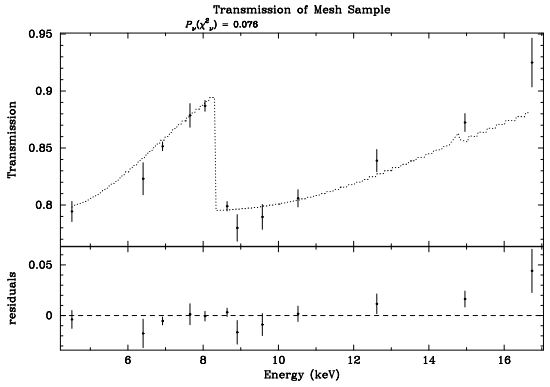

Figure 4. X-Ray transmission of a sample of Ni mesh similar to that in the DMS filter with best-fit model and residuals.

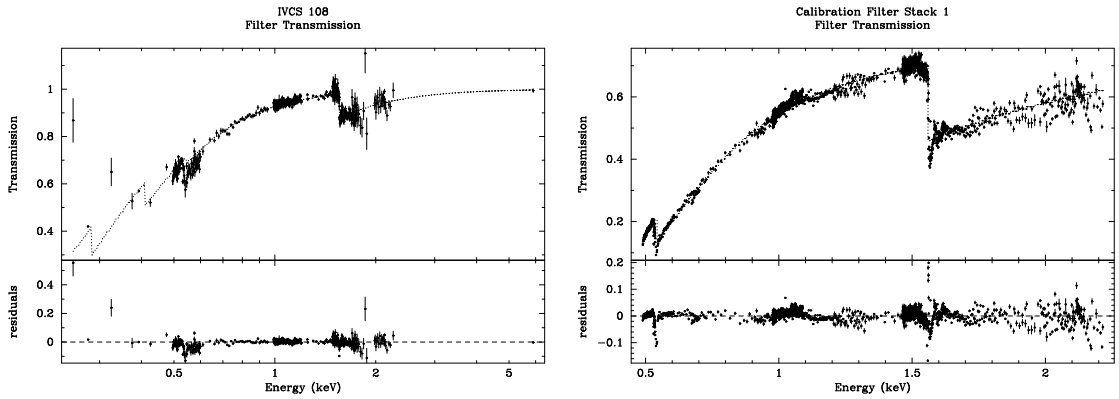

Figure 5. Left: X-Ray transmission of IVCS filter #108. SNR, ES, and GSFC Optics Branch data have been combined. Right: X-Ray transmission of a stack of five calibration filters (one of each type). ES data were taken with the CCD in four different positions to obtain better spectral coverage. In each case the regions near the O and Al edges where fine structure is evident were not included in the fit.

was used, where $M(E)$ is as in Equation 1 when a Ni mesh is present and $M(E) = 1$ otherwise. The mesh thickness, t, width, w and pitch, p were held fixed for these fits, as we do not have any data near the Ni edge to constrain the mesh geometry. The aluminum in the filters is supposed to contain 1% silicon. As we do not have good enough counting statistics to constrain this, $\sigma_{\rm Si}$ was fixed at $0.01\sigma_{\rm Al}$. For the first set of fits we allowed all the other areal densities to be free. The model in Equation 2 does not include the fine structure near the oxygen and aluminum edges so we excluded the edge regions from the fits. The excluded regions were 0.529–0.55 keV and 1.55–1.63 keV. The fitted areal densities are compared with the expected values in Figure 6. For Neon 106 and IVCS 97 the carbon and nitrogen areal densities were not well-constrained by the data due to the lack of data points near these edges.

The DMS filter fits were not good and the DMS 139 ES data did not agree with the GSFC Optics Branch data. Since the beam size at the filter (200×20 μm) is comparable to the mesh parameters (pitch 344 μm and width 40μm) it seemed possible that we were not sampling the mesh properly with the ES. The Optics Branch measurements were done at five different positions with a beam size of a few mm^2 and should not have had this problem.

Thus, to compensate for incomplete sampling of the DMS mesh by the ES beam, we excluded the GSFC Optics Branch measurements from fits to the the DMS filters and Calibration Filter Stack, and allowed the mesh width to vary. In each case the best-fit mesh width was inconsistent with the value derived from the mesh sample (37.5 ± 1.2 μm). DMS 139 was most different with a best-fit mesh width of 28.9 ± 0.4 μm. This explains the obvious discrepancy between the ES measurements and the GSFC Optics Branch measurements. We also fixed the ratio

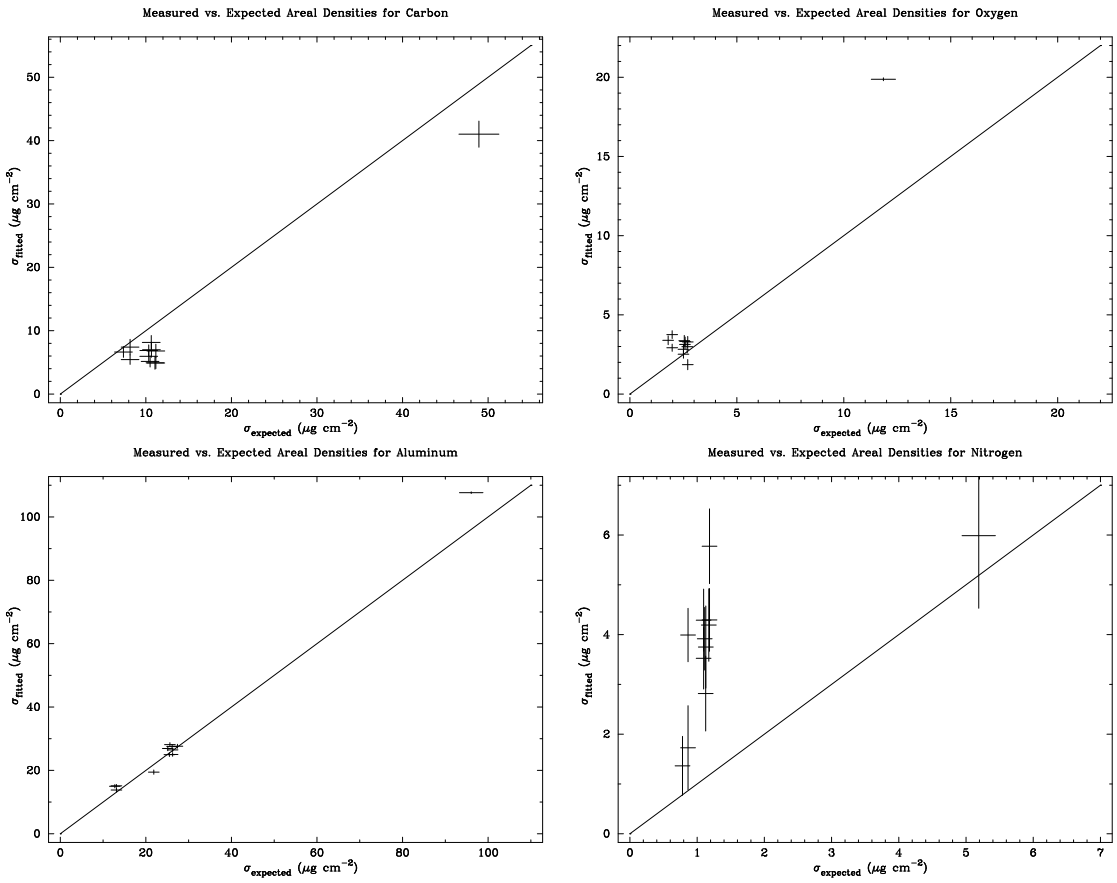

Figure 6. Fitted areal densities vs. expected values for the XRS filters. In these fits all the areal densities were allowed to vary independently except for silicon. The silicon areal density was fixed at 1% of the aluminum value. The solid line is where points would lie if the measured and expected values were the same.

of nitrogen and carbon areal densities at the value expected from the chemical formula of polyimide (0.106 for $C_{22}H_{10}O_4N_2$). The fits were repeated and the results are compared with the expected values in Figure 7.

There is a tendency for the fitted oxygen areal density to be bigger than the expected value listed in Table 3. To see if this extra oxygen was consistent with oxidation of the aluminum of the filters, we calculated the thickness of Al_2O_3 that would would be required to produce the observed excess of measured over expected oxygen areal density, asssuming a density of 3.6 g cm^{-3}. These thicknesses are shown in Table 4. The Calibration Filter Stack measurement is consistent with 112 ± 7 Å of Al_2O_3 per filter.

Table 4. Measured areal densities of the XRS filters. In these fits the ratio of the areal densities of nitrogen to carbon was fixed to the value expected from the chemical formula of polyimide (0.106 for $C_{22}H_{10}O_4N_2$). Again, silicon was fixed at 1% of aluminum. Errors are for 90% confidence in one interesting parameter. The oxide thickness was calculated from the excess of the oxygen areal density over that expected from the Luxel values (see Table 3), assuming a density of 3.6 g cm^{-3} for Al_2O_3.

Filter	Aluminum σ (μg cm^{-2})	Carbon σ (μg cm^{-2})	Oxygen σ (μg cm^{-2})	Oxide Thickness (Å)
DMS 138	21.7 ± 1.7	11.49 ± 0.88	6.06 ± 0.50	202 ± 33
DMS 139	26.4 ± 1.2	11.21 ± 0.56	3.73 ± 0.50	73 ± 33
DMS 156 (Flight)	21.2 ± 1.1	8.22 ± 0.57	2.32 ± 0.51	-21 ± 33
IVCS 97	27.5 ± 3.5	8.5 ± 1.7	3.02 ± 0.34	30 ± 25
IVCS 108	26.65 ± 0.81	12.55 ± 0.52	2.22 ± 0.35	-29 ± 25
IVCS 114	24.73 ± 0.65	8.86 ± 0.44	3.69 ± 0.36	68 ± 26
IVCS 123	27.35 ± 0.71	10.39 ± 0.41	3.23 ± 0.31	38 ± 23
IVCS 143 (Flight)	26.29 ± 0.56	10.10 ± 0.37	2.78 ± 0.27	16 ± 22
Neon 106	25.4 ± 1.2	9.93 ± 0.61	3.80 ± 0.34	75 ± 25
Neon 119	28.01 ± 0.68	10.48 ± 0.41	3.46 ± 0.30	52 ± 23
Neon 146 (Flight)	24.82 ± 0.57	10.07 ± 0.35	3.02 ± 0.31	30 ± 23
Neon 153	27.35 ± 0.68	9.12 ± 0.44	3.62 ± 0.38	54 ± 27
FEA 116	14.99 ± 0.48	9.34 ± 0.32	3.17 ± 0.25	70 ± 21
FEA 117	13.71 ± 0.66	8.50 ± 0.36	3.79 ± 0.25	107 ± 21
FEA 144 (Flight)	14.87 ± 0.52	7.36 ± 0.33	3.44 ± 0.28	98 ± 22
Calibration Stack 1	110.41 ± 0.31	41.51 ± 0.16	21.31 ± 0.12	558 ± 34

As a check on our results, we next fixed the areal densities of aluminum, carbon, and nitrogen at the values expected from the Luxel-quoted aluminum and polyimide thicknesses and repeated the fits. The results are shown in Table 5 and Figure 8. Again, we find that there is excess oxygen. In both cases we find that the Calibration Filter Stack has a much greater oxygen excess than any individual filter, as would be expected since it contains five filters. We find that there is considerable scatter in the oxide thicknesses derived from the individual filter measurements. However, the excess oxygen in the Calibration Filter Stack is again much larger than that in any of the individual filters. For this fit the excess oxygen in the Calibration Filter Stack is consistent with an average of 88 ± 7 Å of Al_2O_3 per filter.

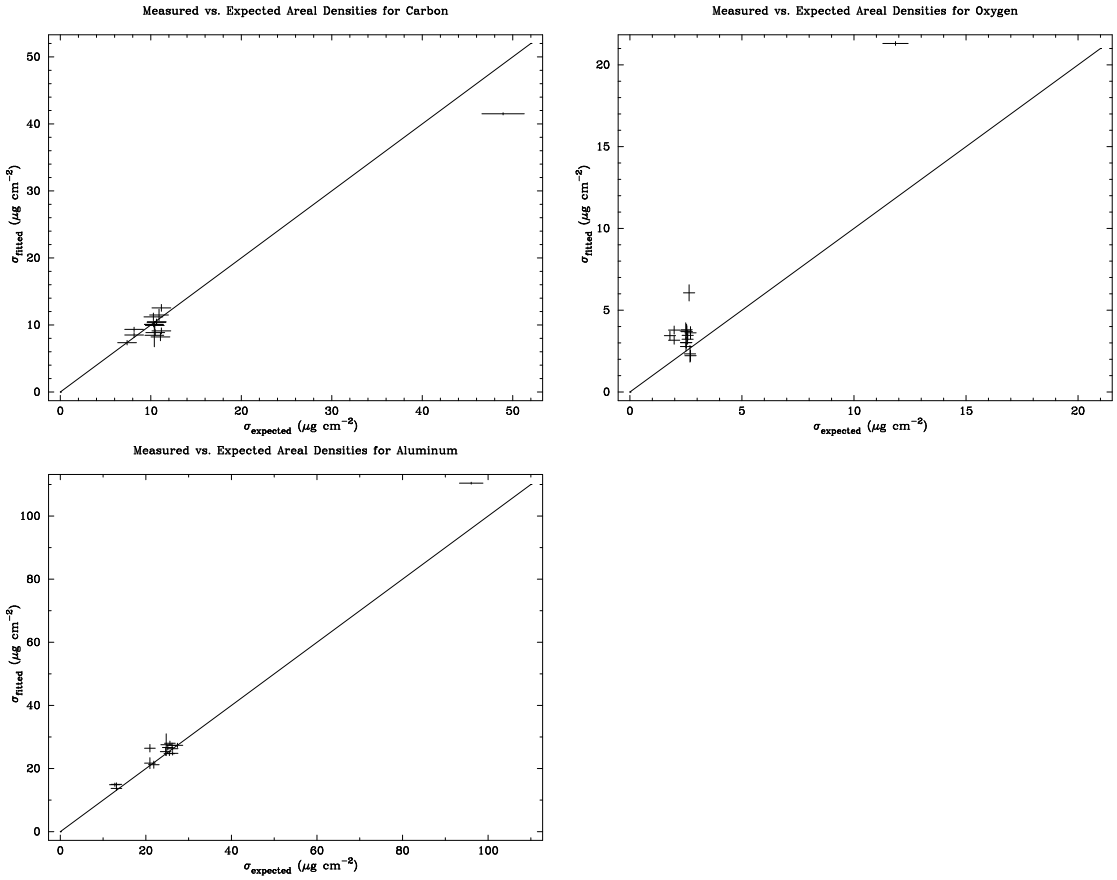

Figure 7. Fitted areal densities vs. expected values for the XRS filters. In these fits the ratio of the areal densities of nitrogen to carbon was fixed to the value expected from the chemical formula of polyimide (0.106 for $C_{22}H_{10}O_4N_2$). Silicon was fixed at 1% of aluminum. The solid line is where points would lie if the measured and expected values were the same.

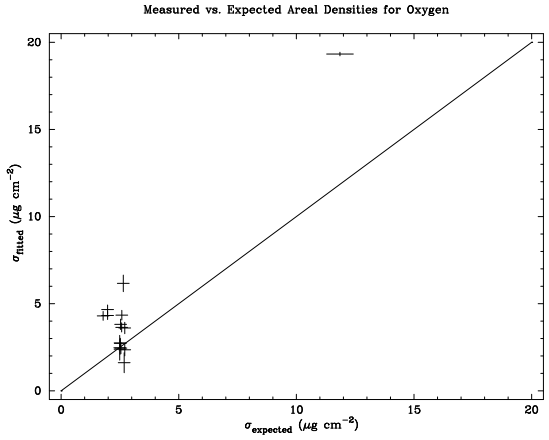

Figure 8. Fitted oxygen areal densities vs. expected values for the XRS filters. In these fits all the areal densities were fixed at the Luxel-derived values, except oxygen and silicon was fixed at 1% of aluminum. The solid line is where points would lie if the measured and expected values were the same.

Table 5. Measured areal densities and estimated oxide thicknesses of the XRS filters. In these fits all the areal densities were fixed at the Luxel-derived values (see Table 3), except oxygen. Errors are for 90% confidence in one interesting parameter. The oxide thickness was calculated from the excess of the oxygen areal density over that expected from the Luxel values, assuming a density of 3.6 g cm^{-3} for Al_2O_3.

Filter	Oxygen σ (μg cm^{-2})	Oxide Thickness (Å)
DMS 138	6.17 ± 0.48	208 ± 32
DMS 139	2.47 ± 0.71	-1 ± 45
DMS 156 (Flight)	1.61 ± 0.57	-63 ± 37
IVCS 97	2.73 ± 0.29	12 ± 23
IVCS 108	3.61 ± 0.33	53 ± 24
IVCS 114	2.45 ± 0.33	-5 ± 24
IVCS 123	3.64 ± 0.26	63 ± 21
IVCS 143 (Flight)	2.75 ± 0.22	14 ± 20
Neon 106	3.82 ± 0.30	76 ± 23
Neon 119	4.34 ± 0.28	104 ± 22
Neon 146 (Flight)	2.39 ± 0.29	-7 ± 23
Neon 153	2.35 ± 0.35	-21 ± 25
FEA 116	4.66 ± 0.26	158 ± 22
FEA 117	4.32 ± 0.23	139 ± 20
FEA 144 (Flight)	4.30 ± 0.25	148 ± 21
Calibration Stack 1	19.33 ± 0.10	441 ± 34

To summarize, we have presented the results of three sets of fits using the model of Equation 2. In Set 1 (see Figure 6), all the areal densities (except silicon which was constrained to be 1% of aluminum) were allowed to vary, the GSFC Optics Branch data were included, and the mesh thickness was fixed for the DMS filters and Calibration Filter Stack. In Set 2 (see Figure 7 and Table 4), the ratio of carbon to nitrogen was fixed at the value expected for polyimide and, for the DMS filters and Calibration Filter Stack, the GSFC Optics Branch data were excluded and the mesh thickness was allowed to vary. In Set 3 (see Figure 8 and Table 5), all the areal densities except oxygen were fixed at the expected values listed in Table 3. Again, for the DMS filters and Calibration Filter Stack, the GSFC Optics Branch data were excluded and the mesh thickness was allowed to vary.

For each set of fits we find excess oxygen. For set 1 the estimated oxide thickness for the Calibration Filter Stack was 473 ± 34 Å, or 95 ± 7 Å per filter. For set 2 it was 558 ± 34 Å, or 112 ± 7 Å per filter. For set 3 it was 441 ± 34 Å, or 88 ± 7 Å per filter. In Figure 7 the carbon and aluminum areal densities are close to the expected values. This, and the fact that we are measuring the areal densities more precisely than Luxel, leads us to have most confidence in the results of set 2.

4. FUTURE PLANS

We continue to measure filter transmissions with the ES and our analysis is ongoing.

We intend to investigate the temperature dependence of EXAFS in the engineering model filters by cooling them to liquid helium temperatures. We expect to see two temperature-related effects. The decrease in lattice spacing with cooling will change the observed spacing of features in the edge fine structure. Also, as thermal noise is reduced, these features will become sharper. Knowledge of this temperature dependence is essential as the various filters will be at temperatures ranging from 60 mK to 200 K.

5. CONCLUSIONS

The nickel mesh of the DMS filter is not optically thick to X-rays. This provides an unexpected boon for calibration. By observing the Ni edge in the spectra from bright sources we will be able to constrain the high-energy gain of XRS. Lack of knowledge of the XRS gain function at high energies could otherwise have been a problem.[3]

We have detected excess oxygen which is consistent with self-limiting oxidation of the aluminized coatings of the filters. We find average of 112 ± 7 Å of Al_2O_3 per filter. This result is tentative, however, and may be affected by systematic errors. As we obtain more data we hope to refine this value.

ACKNOWLEDGMENTS

We would like to thank Mike Hettrick, Dale Arbogast, and Alan Crane.

REFERENCES

1. Y. Ogawara, "The ASTRO-E mission," in *Proceedings of IAU Symposium no 188*, Kyoto, 1998.
2. R. L. Kelley *et al.*, "The ASTRO-E/XRS high resolution x-ray spectrometer," in *Proc. SPIE,*, vol. 3765, 1999.
3. K. C. Gendreau, M. D. Audley, K. A. Arnaud, K. R. Boyce, R. Fujimoto, Y. Ishisaki, R. L. Kelley, T. Mihara, K. Mitsuda, F. S. Porter, C. K. Stahle, and A. E. Szymkowiak, "The ASTRO-E/XRS calibration program and results," in *Proc. SPIE,*, vol. 3765, 1999.
4. B. M. McLaughlin and K. P. Kirby, "Photoabsorption of atomic oxygen in the vicinity of the K-edge," *J. Phys. B,* **31**, p. 4991, 1998.
5. M. C. Hettrick, "Surface normal rotation: a new technique for grazing incidence monochromators," *Appl. Opt.,* **31**, p. 7174, 1992.
6. M. C. Hettrick and S. Bowyer, "Variable line-space gratings: new designs for use in grazing incidence spectrometers," *Appl. Opt.* **22**, p. 3221, 1983.
7. M. C. Hettrick, S. Bowyer, R. F. Malina, C. Martin, and S. Mrowka, "Extreme ultraviolet explorer spectrometer," *J. Opt. Soc. Am.* **68**, p. 1106, 1978.
8. B. L. Henke, E. M. Gullikson, and J. C. Davis, "X-ray interactions: photoabsorption, scattering, transmission, and reflection at E=50–30000 eV, Z=1–92," *Atomic Data and Nuclear Data Tables,* **54**, pp. 181–342, July 1993.